Effect of Ternary Additions on the Stability of Ordered Phases in Ni-Mo Alloys—Transmission Electron Microscopy Results and First Principles Calculations

A. ARYA, U.D. KULKARNI, G.K. DEY, and S. BANERJEE

The ordering behavior of a Ni-Mo alloy in the presence of ternary additives X (X = Al, Cr, Mn, V) has been studied using transmission electron microscopy (TEM) as well as first-principles calculations using the tight-binding–linear muffin tin orbital (TB-LMTO) method. The sequence of ordering transformations in binary Ni-Mo alloys has been shown earlier to be controlled by a competition between several fcc-based superlattices, *viz*. Ni_2Mo (Pt_2Mo type), Ni_3Mo ($D0_{22}$), Ni_4Mo ($D1_a$), and the so-called short-range ordered (SRO) structure characterized by the presence of $\{1\frac{1}{2}0\}$ reflections. These ternary additives have been observed to stabilize the Ni_3Mo ($D0_{22}$) phase compared to the Ni_2Mo + Ni_4Mo phase mixture, leading to a sequence of transformation different from that obtained in binary alloys. The calculated energies of formation were observed to conform to the experimentally observed stability hierarchy in these binary intermetallics and their ternary analogues. The third element stabilizes the $D0_{22}$ structure by contributing to the covalent component of bonding in these compounds.

DOI: 10.1007/s11661-007-9362-8

I. INTRODUCTION

ORDERING transformations in Ni-Mo alloys and their ternary derivatives show several interesting features. Considerable transmission electron microscopy (TEM) and theoretical work has been carried out on these alloys over the last four decades.[1–19] Significant controversy exists in the literature, pertaining mainly to the nature and the origin of the quenched-in short-range-ordered (SRO) state in Ni-rich binary alloys and to the evolution of the long-range-ordered (LRO) phases from the state of SRO.

Intensity maxima at $\{1\frac{1}{2}0\}$ and equivalent positions in the reciprocal space and the appearance of streaks of diffuse intensity of various shapes joining the positions of the SRO maxima and the superlattice positions of the LRO phases are some of the distinguishing characteristics of the initial stages of ordering in binary Ni-Mo.

An interesting aspect of the ordering transformations is the way the nature of the SRO state and the stability of the LRO phases that result is altered by small amounts of ternary additions to Ni-Mo.[9,10,18] Partial replacement of Mo with Al,[18] for instance, results in a state of SRO that shows $\{100\}$ and equivalent SRO maxima in addition to the $\{1\frac{1}{2}0\}$ and equivalent maxima evidenced in the case of the binary alloy. As both types of static concentration waves (with wave vectors $\mathbf{k_1} = \{100\}$ and $\mathbf{k_2} = \{1\frac{1}{2}0\}$) are simultaneously present, this state is akin to a SRO $D0_{22}$ structure.[18,19]

There has been a great deal of interest in studying the effect of ternary additions (*e.g.*, Cr, V, Ta, *etc.*) on the ordering behavior of these alloys.[20–23] A partial substitution of Mo by elements with $e/a < 6$, which reduces the overall e/a ratio to 8.75, stabilizes the $D0_{22}$ structure *vis-à-vis* the phase mixture of $D1_a$ and Pt_2Mo-type structures. A further decrease in the e/a ratio to 8.25 stabilizes the $L1_2$ structure. However, no explanation was given for this preference in a rigorous manner. On the other hand, the general tendency of the Ni_3Mo alloy and some of its ternary derivatives to decompose into a mixture of the Ni_2Mo and the Ni_4Mo phases, avoiding the $D0_{22}$ structure, which satisfies the stoichiometry, has been rationalized in terms of nearly equal stabilities associated with the competing structures.[3]

An important point regarding the stability of ordered phases in Ni-Mo-X alloys (where X refers to a third element such as Al, Cr, Mn, or V) is that the LRO state of the *binary* alloy of Ni_3Mo composition comprises a phase mixture of Ni_4Mo ($D1_a$) and Ni_2Mo (Pt_2Mo-type). The stoichiometric Ni_3Mo ($D0_{22}$) phase appears only in alloys wherein Mo is partially substituted by Al,[9,10,18] Cr (References 22 and 25, and references therein) or Mn.[26] In the binary alloy, the phase mixture is present over the entire composition range from Ni_4Mo to Ni_2Mo. In the aforementioned ternary alloys, however, a mixture of either $D1_a$ and $D0_{22}$ over the composition range Ni_4Y to Ni_3Y (where Y is Mo + X)) or $D0_{22}$ and Pt_2Mo over the composition range Ni_3Y to Ni_2Y has been observed. The problem of stability of coherent ordered phases in Ni-Mo-X alloys thus boils

A. ARYA, U.D. KULKARNI, G.K. DEY, and S. BANERJEE, Scientists, are with the Materials Science Division, Bhabha Atomic Research Centre, Mumbai 400 085, India. Contact e-mail: ashokarya@gmail.com

This article is based on a presentation given in the symposium entitled "Materials Behavior: Far from Equilibrium" as part of the Golden Jubilee Celebration of Bhabha Atomic Research Centre, which occurred December 15–16, 2006 in Mumbai, India.

Article published online December 4, 2007

down to a simple question—What is the LRO state at Ni_3Y composition? Is it $D0_{22}$ or is it the phase mixture of $D1_a$ and Pt_2Mo?

First-principles electronic structure calculations on binary Ni-Mo alloy has been investigated earlier[24] in the entire composition range using the tight-binding linear muffin tin orbital (TB-LMTO) method. These calculations confirmed the higher stability of Ni_2Mo + Ni_4Mo phase mixture over that of Ni_3Mo ($D0_{22}$ or $L1_2$) phase and also verified the experimentally observed orthorhombic $D0_a$ (*Pmmn*) phase to have lower formation energies (and hence higher stability) compared to the $D0_{22}$ phase. The effect of ternary (Cr) addition on long-range ordering of Ni-Mo alloys has also been investigated in terms of relative formation energies calculated from first-principles full-potential linear augmented plane wave (FLAPW) calculations[25] using the supercell approach. These calculations showed that Cr contributes to the bonding strength in the ternary $D0_{22}$ phase; whereas in the ternary $D1_a$ and Pt_2Mo-type superstructures, it has the effect of weakening the bonds compared to the binary analogues. The selection of the ternary element and its concentration is expected to have a strong influence on the relative phase stabilities of the competing superlattice structures. With this in mind, we have investigated the effect of four ternary additives, *viz*. Al, Cr, Mn, and V, on the relative phase stability of $D0_{22}$, $D1_a$, and Pt_2Mo-type intermetallics using a first-principles electronic structure method and compared our calculated stability sequence with that observed experimentally using TEM.

In the next section, we summarize the methodology of our first-principles based calculations. Next, we present our results in two parts: the first part deals with the transmission electron microscopy (TEM) and high-resolution TEM studies on the ordering behavior of ternary Ni-Mo-X (X = Al, Cr, Mn, and V) alloys. The second part involves first-principles local-density based TB-LMTO calculations of ground state stabilities of binary and ternary phases crystallizing into three possible structures having space groups *Immm* (Ni_2Mo), *I*4/*mmm* (Ni_3Mo), and *I*4/*m* (Ni_4Mo), respectively. The relative ground state stabilities of all these superstructures have been compared with that observed experimentally and a discussion has been presented on the ordering behavior of the Ni-Mo alloy in the presence of these ternary additives.

II. FIRST-PRINCIPLES CALCULATIONS

Density functional theory (DFT)[27,28] is now a well established tool for accurate description of the electronic structures of solids. Electronic structure calculations have been performed using the first-principles TB-LMTO method,[29–31] which combines the simplicity of the TB approach with the accuracy comparable to that of the Korringa–Kohn–Rostoker (KKR) method. For close-packed metallic systems, the simplifying atomic sphere approximation (ASA)[31] has proved to be quite successful. In the case of binary intermetallics, if there is considerable size difference between the two constituents (as in the Ni-Mo system under consideration here), it is desirable to ensure that the overlap between the atomic spheres of radii s_1 and s_2, defined as $100*(s_1 + s_2 - d)/s_1$, remains less than ~30 pct. The errors due to neglect of the interstitial region and truncation of higher partial waves are minimized by incorporating the so-called "combined correction" terms. According to Andersen,[30] ASA with combined correction should yield reasonable accurate results especially for close-packed intermetallics. We have used the von Barth–Hedin parameterization[32] of the exchange-correlation potential in our local density band calculations. In our calculation, *s*-, *p*-, and *d*-partial waves have been used (*i.e*., maximum angular momentum $l_{max} = 2$), and the *f*-orbitals have been downfolded. Finally, the tetrahedron method for the Brillouin zone (*i.e*., **k**-space) integrations has been used with its latest version, which avoids misweighting and corrects errors due to the linear approximation of the bands inside each tetrahedron. The calculations were fully converged with respect to the number of **k**-points.

For our calculations, we have taken three binary intermetallic structures, *viz*. Pt_2Mo-type Ni_2Mo (*Immm*), $D0_{22}$-Ni_3Mo (*I*4/*mmm*), and $D1_a$-Ni_4Mo (*I*4/*m*) and their ternary analogues (Ni-Mo-X, X = Al, Cr, Mn, and V), *viz*. $Ni_{16}Mo_6X_2$ (*Immm*), $Ni_{24}Mo_6X_2$ (*I*4/*mmm*), and $Ni_{32}Mo_6X_2$ (*I*4/*m*), respectively. The relevant consideration for selecting these ternary compositions was to have equal distribution of the third element (X) in the Ni_3Mo phase and the Ni_2Mo + Ni_4Mo phase mixture for the purpose of comparing their stabilities. The unit cells of these ternary analogues were generated using a "supercell" approach, in which a $2 \times 2 \times 2$ supercell of a given ternary phase was created from the corresponding binary unit cells (Figure 1). Then, selectively, some of the Mo sublattice sites were substituted by the species X to correspond to given atomic fractions. The substitution of only the Mo site by the ternary additives is based upon observed experimental evidence.

Self-consistent calculations were performed on the preceding phases to obtain total energy (E_T) as a function of volume (V) to obtain equilibrium cohesive properties, *viz*. equilibrium volume (V_0) or lattice parameter, bulk modulus, and the energy of formation (E_{FORM}). The free atom calculations were performed semirelativistically, using the same computer code as was used for our solid calculations, but with a large cutoff ($r_{max} = 30$ a.u.).

III. RESULTS AND DISCUSSION

A. *Experimental Results*

1. *Ordering in binary Ni-Mo alloys*

The quenched-in state of SRO in binary Ni-Mo shows the intensity maxima at only {1½0} and equivalent positions. A complete absence of intensity is noticed at {100} and equivalent positions. Thus, this means that the state of SRO is significantly different from what one would expect to be the initial stage of formation of a $D0_{22}$ structure as the $D0_{22}$ would give rise to intensity

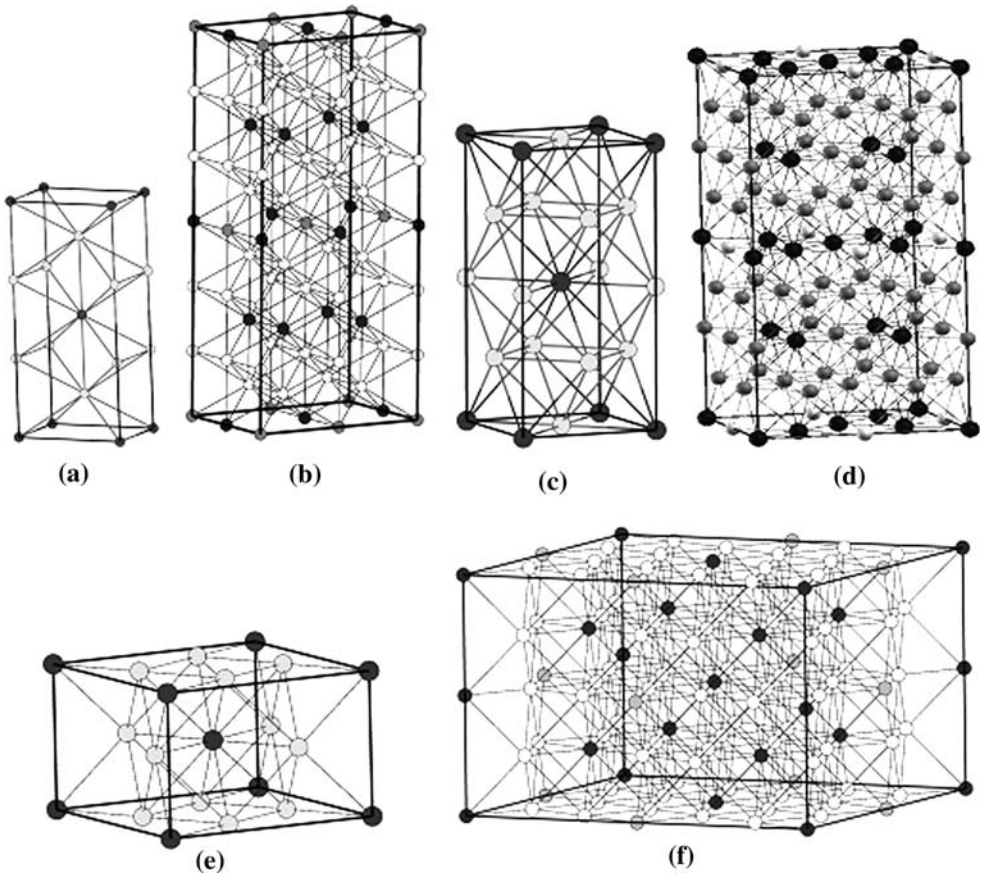

Fig. 1—Unit cells of (*a*) Ni_2Mo (*Immm*) and (*b*) its supercell ($Ni_{16}Mo_6X_2$); (*c*) Ni_3Mo (*I*4/*mmm*) and (*d*) its supercell ($Ni_{24}Mo_6X_2$); and (*e*) Ni_4Mo (*I*4/*m*) and (*f*) its supercell ($Ni_{32}Mo_6X_2$). Ni: gray circles, Mo: dark circles, and X: white circles.

maxima (or superlattice reflections) at both {1½0} and equivalent and {100} and equivalent positions. The atomic structure of such a state of SRO has been a subject of considerable controversy. Recent Monte Carlo simulations[16,19] throw some light on its complex nature.

On prolonged aging, an alloy of Ni_4Mo composition yields microdomains corresponding to six different variants of $D1_a$. An alloy of Ni_3Mo composition, on the other hand, separates into a phase mixture of Ni_4Mo ($D1_a$) and Ni_2Mo (Pt_2Mo-type) ordered phases. Sharp $^1_3\{220\}$ and equivalent superlattice reflections of Pt_2Mo and $^1_5\{420\}$ and equivalent superlattice reflections of $D1_a$ can then be seen (Figure 2(a)) in the selected area electron diffraction patterns (SAEDPs).

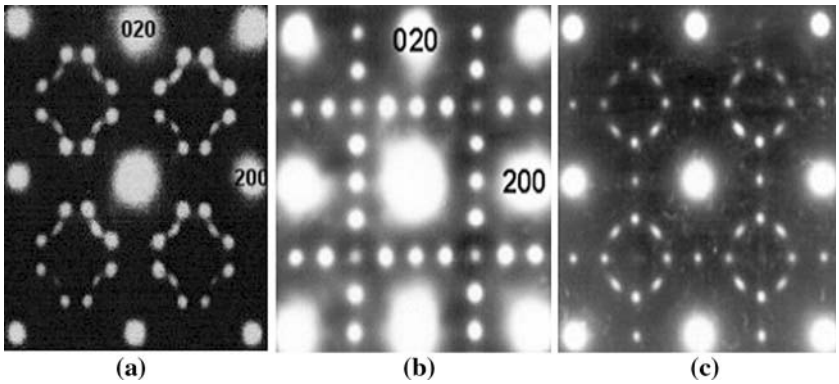

Fig. 2—[001] SAEDPs (*a*) from a binary Ni_3Mo alloy showing superlattice reflections arising from two different variants each of Ni_4Mo ($D1_a$) and Ni_2Mo (Pt_2Mo type). Note the elongated nature of the $^1_3\{220\}$ of Pt_2Mo reflections. (*b*) SRO state in $Ni_{70}Mo_{25}Al_5$, which shows intensity maxima at both {1½0} and equivalent and {100} and equivalent positions. (*c*) On prolonged aging, the $Ni_{70}Mo_{25}Al_5$ alloy decomposes into a mixture of $D0_{22}$ and Pt_2Mo-type LRO phases. Superlattice reflections from two different variants of each of these phases can be seen in the SAEDP. Please refer to the key to these [001] SAEDPs shown in Fig. 3.

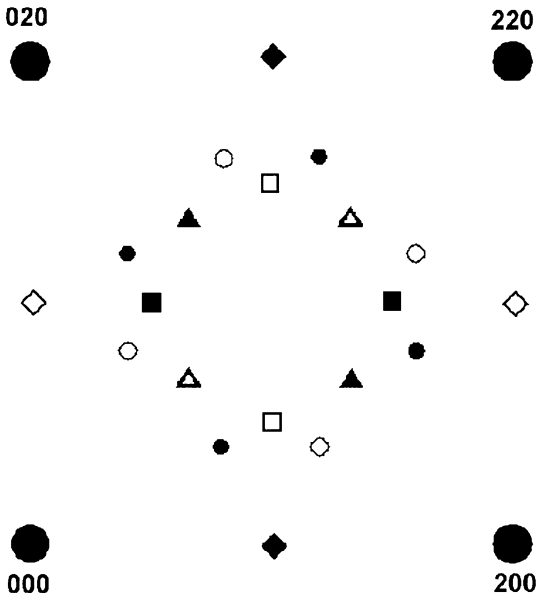

Fig. 3—Key showing the positions of superlattice reflections in [001] SAEDPs. ●—Fundamental fcc reflections, ■ □—{1½0} and equivalent $D0_{22}$ reflections and SRO maxima, ◆ ◇—{100} and equivalent $D0_{22}$ reflections, ▲ △—Pt_2Mo reflections, and ● ○ —$D1_a$ reflections. The solid and the open symbols correspond to different variants of the structures. {110} reflections arise from a third $D0_{22}$ variant with its *c*-axis parallel [001].

2. *Ordering in $Ni_{70}Mo_{25}Al_5$ alloy*

The SRO state of the alloy clearly represents an early stage of evolution of LRO $D0_{22}$. Intensity maxima can be seen to be present in the superlattice positions of three different $D0_{22}$ variants (Figure 2(b)). The Al addition to Ni-Mo thus gives rise to a modified state of SRO with intensity maxima at both {1½0} and equivalent and {100} and equivalent positions in the fcc reciprocal space. Because the (Mo + Al) content of the alloy, referred to as Y earlier, is about 0.3, prolonged aging results in a mixture of LRO $D0_{22}$ and Pt_2Mo-type phases. Sharp superlattice reflections from both of these phases can be seen to be present in the SAEDP in Figure 2(c).

3. *Ordering in $Ni_{75}Mo_{20}Mn_5$ alloy*

The effect of Mn addition appears to be quite similar to that of Al. The Mn containing alloy also shows a state of SRO that appears to be a precursor to LRO $D0_{22}$. It shows intensity maxima at both {1½0} and equivalent and {100} and equivalent positions. On prolonged aging, the alloy develops LRO $D0_{22}$ structure. This is due to the fact that the (Mo + Mn) content of the alloy is close to 0.25. It, therefore, is quite close in stoichiometry to $D0_{22}$. Large antiphase domains belonging to a single $D0_{22}$ variant can be seen in Figure 4(b), and the corresponding [001] SAEDP shows superlattice reflections from a single variant of the phase.

B. *Calculational Results*

Tables Ia and Ib summarize the ground state equilibrium cohesive properties, *viz*. equilibrium lattice parameter, bulk modulus, and energy of formation (E_{form}), of elemental solids in the Ni-Mo-X alloy system and their intermetallic phases, respectively, calculated using the TB-LMTO-ASA method under the local-density approximation along with their reported experimental results[32–34] as well as those calculated using the full-potential linear augmented plane wave (FLAPW) method[25] for comparison. As can be seen from Table Ia, the calculated equilibrium lattice parameters (or volume) of all the elemental phases show an excellent (< 1 pct) match with both experimental and FLAPW results, though the calculated values are systematically underestimated with respect to the experimental results, which is due to the use of ASA, which invariably slightly overestimates bonding. Here, it should be noted that we have performed spin-polarized calculations for Ni and Cr, where the ground state of Cr has been taken to be antiferromagnetic. For Mn, the ground state has been taken to be a Mn(α) structure having a space group, $I\bar{4}3m$, with 29 atoms in its unit cell.[33] Similarly, for binary intermetallics (Table Ib), the TB-LMTO calculated lattice parameters are slightly lower than those calculated using the FLAPW method.[25]

The bulk modulus (*B*), obtained from the second derivative of the total energy with respect to volume,

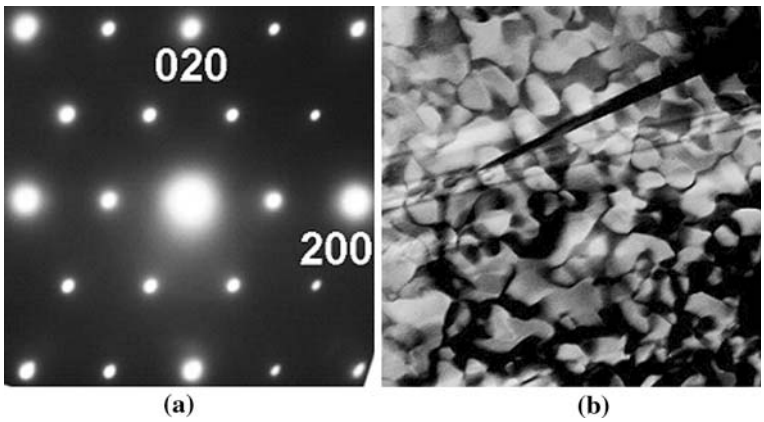

Fig. 4—(*a*) [001] SAEDP showing superlattice reflections from a single $D0_{22}$ variant with its *c*-axis parallel to [100] of fcc. (*b*) A dark-field image showing large $D0_{22}$ antiphase domains.

Table Ia. LMTO-ASA-LDA Calculated Ground State Equilibrium Cohesive Properties of Elements in the Ni-Mo-X System; the Numbers Given in Box Brackets are the Experimental Results,[35] Whereas Those in Braces are the FLAPW Results[25]

System	Lattice Parameter (a) (Å)	Bulk Modulus (GPa)	Energy of Formation (eV/atom)	DOS at Fermi Level ((eV·atom)$^{-1}$)
Ni (fcc)	3.4545 [3.524] {3.5117}	254.2 [186.0] {248.90}	0.000	0.184 (↑) 1.550 (↓)
Mo (bcc)	3.1263 [3.1470] {3.1530}	286.8 [261] {254.73}	0.000	0.578
Al (fcc)	3.9950 [4.048]	85.8 [75.2]	0.000	0.307
Cr (bcc)	2.8338 [2.882] {2.8232}	289.2 [190.0] {267.81}	0.000	0.709
Mn (I-43m)	8.8911 [8.9126]	308.5	0.000	1.198
V (bcc)	2.9705 [3.024]	205.3 [161.9]	0.000	1.854

Table Ib. LMTO-ASA-LDA Calculated Ground State Equilibrium Cohesive Properties of Binary and Ternary Intermetallics in the Ni-Mo System; the Numbers Given in Box Brackets are the Experimental Results,[35] Whereas Those in Braces are the FLAPW Results.[25] For Body-Centered Orthorhombic $Ni_2(Mo, X)$ Intermetallics, the b/a and c/a Ratios are 1.414 and 3.000, Respectively, Whereas for Body-Centered Tetragonal $Ni_3(Mo, X)$ and $Ni_4(Mo, X)$ Intermetallics, the c/a Ratios are 2.000 and 0.633, Respectively

System	Lattice Parameter (a) (Å)	Bulk Modulus (GPa)	Energy of Formation (eV/atom)	DOS at Fermi level ((eV·atom)$^{-1}$)
Ni_2Mo (Pt_2Mo)	2.5582 {2.6522}	269.6 {250.0}	–0.231	0.625
Ni_4Mo ($D1_a$)	5.5825 {5.8200}	278.2 {287.7}	–0.244	1.501
Ni_3Mo ($D0_{22}$)	3.5694 {3.6849}	283.0 {251.6}	–0.220	1.037
$Ni_{16}Mo_6Al_2$	5.0949	251.3	–0.216	1.105
$Ni_{32}Mo_6Al_2$	11.1381	264.2	–0.279	1.112
$Ni_{24}Mo_6Al_2$	7.1121	265.4	–0.320	0.654
$Ni_{16}Mo_6Cr_2$	5.0673	266.3	–0.151	0.732
$Ni_{32}Mo_6Cr_2$	11.1136	281.0	–0.186	1.361
$Ni_{24}Mo_6Cr_2$	7.0996	293.1	–0.173	0.901
$Ni_{16}Mo_6Mn_2$	5.0572	313.0	–0.143	0.675
$Ni_{32}Mo_6Mn_2$	11.1037	277.0	–0.175	1.234
$Ni_{24}Mo_6Mn_2$	7.0921	289.4	–0.163	0.832
$Ni_{16}Mo_6V_2$	5.0871	263.4	–0.164	0.651
$Ni_{32}Mo_6V_2$	11.1339	312.4	–0.244	1.032
$Ni_{24}Mo_6V_2$	7.1133	283.8	–0.249	0.741

generally has large error bars. The bulk modulus has been calculated by fitting total energy into the Murnaghan equation of state.[35] As can be seen in Table Ia, the calculated bulk moduli for Ni, Cr, and V are much larger than the corresponding experimental results, but are comparable with the FLAPW results. For Al and Mo, the bulk moduli agree (within 10 pct) with the experimental results. For intermetallic phases (Table Ib), the calculated bulk moduli fall within a narrow range (251 to 313 GPa), and the values are in good agreement with the FLAPW results, wherever available.

The energy of formation (E_{form}) of a given intermetallic is calculated by subtracting the weighted sum of cohesive energies of constituent elements from the cohesive energy of the intermetallic. The cohesive energy values of elemental phases are calculated to be 8.169, 11.362, 4.227, 7.511, 8.511, and 8.410 eV/atom for Ni, Mo, Al, Cr, Mn, and V, respectively. Here, it should be noted that the systematic errors in cohesive energy values are more or less cancelled for close-packed metallic systems, when we calculate the energy of formation. Our calculated values of E_{form} of all the intermetallic phases are listed in groups in Table Ib. The question of whether it is $D0_{22}$ or it is the phase mixture of $D1_a$ and Pt_2Mo can now be answered by comparing $E_{form}(Ni_3(Mo, X))$ and the sum of $E_{form}(Ni_4(Mo, X))$ and $E_{form}(Ni_2(Mo, X))$, where X = Al, Cr, Mn, and V. For binary Ni-Mo (Table Ib), it can be seen that $E_{form}(Ni_3Mo)$ is greater than $E_{form}(Ni_4Mo) + E_{form}(Ni_2Mo)$, indicating that a phase mixture $D1_a + Pt_2Mo$ will be more stable than the $D0_{22}$ phase. For all ternary intermetallics, one can observe that $E_{form}(Ni_3(Mo, X)) < \{E_{form}(Ni_4(Mo, X)) + E_{form}(Ni_2(Mo, X))\}$, indicating that the ternary $D0_{22}$ phase is energetically favored as compared to the phase mixture of $D1_a$ and Pt_2Mo structures in all the ternary analogues. The effect of the ternary addition (Al, Cr, Mn, V) is, thus, seen to stabilize the $D0_{22}$ structure, and the tendency of the third element for stabilizing the $D0_{22}$ structure is observed to be strongest in the case of Al followed by V, as evidenced by their relative values of energy of formation.

The addition of the third element modifies the nature of the bonding operative in the binary intermetallics, as can be seen in Figure 5, where we have plotted total and *site*- and *l*-projected density of states (DOS) for binary intermetallics (Figure 5(a)) and those of ternary analogues with Al as the third element (Figure 5(b)). For the sake of brevity, we have restricted our interpretation of the change in nature of bonding to the addition of Al

only. The occupied part of the valence DOS plots reveals a multipeaked structure (bandwidth ~9.0 eV) for almost all the binary compounds that are dominated by a Ni-*d* (with a nearly filled *d* band) and Mo-*d* DOS (with a nearly half-filled *d* band). For corresponding ternary analogues, the occupied part of the valence band has a bandwidth of nearly 9.7 eV. In binary compounds, the lower part of the valence band is dominated by Ni-*s* (Figure 5(a)). The mixing of *d*-*d* states is responsible for metallic bonding in these binary intermetallics, as also evidenced by DOS at the Fermi level, $\rho(E_F)$ (Table Ib). The higher the $\rho(E_F)$, the more metallic is the bonding. In the case of Ni-Mo-Al ternary intermetallics, the occupied part of DOS (Figure 5(b) has broadened a little (by ~0.7 eV) as compared to their binary analogues, and the lower part of the valence band exhibits larger mixing of Ni-*s* and Al-*p* states in the $D0_{22}$ structure than that in the $D1_a$ structure. This mixing imparts covalent character to bonding, as also evidenced by comparing $\rho(E_F)$ values for the binary and the

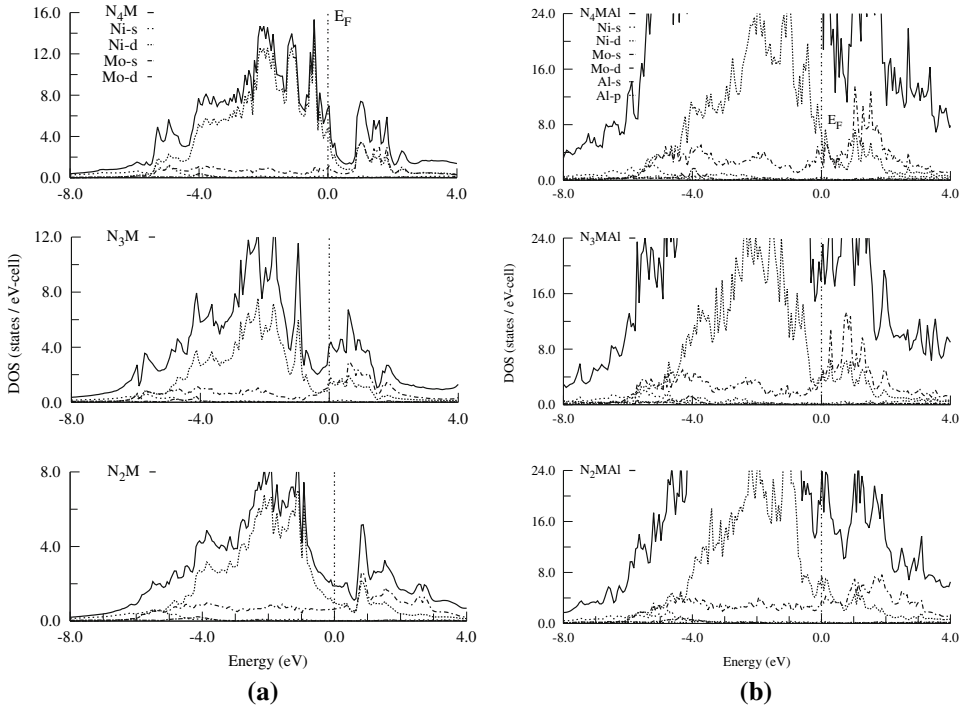

Fig. 5—Total *site*- and *l*-projected DOS for (*a*) binary Ni-Mo intermetallics, where only *s* and *d* states of both Ni and Mo atoms are shown, and for (*b*) ternary Ni-Mo-Al, where partial densities of Ni-*s*, Ni-*d*, Mo-*d*, and Al-*p* states are shown. Mo-*s* and Al-*s* states are not shown here, because their contribution to bonding is either negligible or does not change much in going from the binary to ternary system.

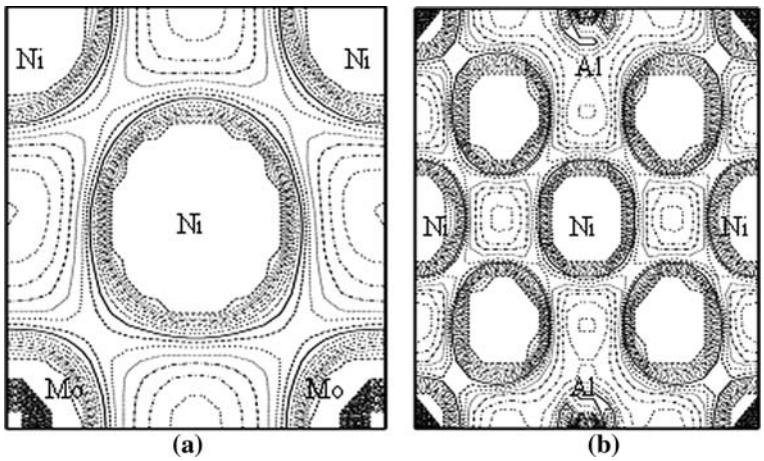

Fig. 6—Valence charge density contour plots, ranging between 0.001*e* to 0.1*e*, on the (100) plane in binary Ni_3Mo ($D0_{22}$) and (b) its ternary superstructure $Ni_{24}Mo_6Al_2$. The enhanced charge density along the Ni-Al bond in (b) reflects the covalent character of the bonding on Al addition.

corresponding ternary analogues, which shows a greater decrease for $D0_{22}$ structures (from 1.037 to 0.654 $(eV{\cdot}atom)^{-1}$) as compared to that in the $D1_a$ structures, while the Pt_2Mo structure shows an increase in $\rho(E_F)$ on adding Al. Similarly, the valence charge density contour plots on the (100) plane of binary Ni_3Mo ($D0_{22}$) and its ternary superstructure $Ni_{24}Mo_6Al_2$ (Figure 6) clearly distinguish the nature of the bonding operative in these two systems. While in binary Ni_3Mo, there is metallic σ *d-d* interactions, the ternary analogue exhibits enhanced charge density along the Ni-Al bond. Thus, it may be concluded that Al stabilizes the $D0_{22}$ structure by contributing to covalent bonding in the ordered phase.

REFERENCES

1. C.R. Brooks, J.E. Sprueill, and E.E. Stansbury: *Int. Metall. Rev.*, 1984, vol. 29, pp. 210–48.
2. E. Ruedl, P. Delavignette, and S. Amelinckx: *Phys. Status Solidi*, 1968, vol. 28, pp. 305–28.
3. S.K. Das, P.R. Okamoto, P.M. Fisher, and G. Thomas: *Acta Metall.*, 1973, vol. 21, pp. 913–28.
4. S.K. Das and G. Thomas: *Phys. Status Solidi (a)*, 1974, vol. 21, pp. 177–90.
5. B. Chakravarti, E.A. Starke, Jr., C.J. Sparks, and R.O. Williams: *J. Phys. Chem. Solids*, 1974, vol. 35, pp. 1317–26.
6. R. de Ridder, G. Van Tendeloo, and S. Amelinckx: *Acta Cryst.*, 1976, vol. A32, pp. 216–24.
7. J.P. Chevalier and W.M. Stobbs: *Acta Metall.*, 1979, vol. 27, pp. 1197–217.
8. G. Van Tendeloo, S. Amelinckx, and D. de Fontaine: *Acta Cryst.*, 1985, vol. B41, pp. 281–92.
9. P.L. Martin and J.C. Williams: *Acta Metall.*, 1984, vol. 32, pp. 1681–93.
10. P.L. Martin and J.C. Williams: *Acta Metall.*, 1984, vol. 32, pp. 1695–702.
11. U.D. Kulkarni and S. Banerjee: *Acta Metall.*, 1988, vol. 36, pp. 413–24.
12. U.D. Kulkarni, S. Muralidhar, and S. Banerjee: *Phys. Status Solidi (a)*, 1988, vol. 110, pp. 331–45.
13. S. Banerjee, U.D. Kulkarni, and K. Urban: *Acta Metall.*, 1989, vol. 37, pp. 35–48.
14. U.D. Kulkarni, G.K. Dey, and S. Banerjee: *Scripta Metall.*, 1988, vol. 22, pp. 437–40.
15. U.D. Kulkarni: *Phys. Rev. Lett.*, 1989, vol. 63, pp. 2484–87.
16. S. Hata, S. Matsumura, N. Kuwano, and K. Oki: *Acta Mater.*, 1998, vol. 46, pp. 881–92.
17. S. Hata, S. Fujita, C.G. Schlesier, S. Matsumura, N. Kuwano, and K. Oki: *Mater. Trans. JIM*, 1998, vol. 39, pp. 133–38.
18. U.D. Kulkarni and G.K. Dey: *Acta Mater.*, 2004, vol. 52, pp. 2711–20.
19. U.D. Kulkarni: *Acta Mater.*, 2004, vol. 52, pp. 2721–32.
20. M. Yamamoto, F. Shohno, and S. Nenno: *Trans. Jpn. Inst. Met.*, 1978, vol. 19, pp. 475–82.
21. M. Yamamoto, N. Soji, T. Sabury, and Y. Mizutani: *Trans. Jpn. Inst. Met.*, 1970, vol. 11, pp. 120–27.
22. S. Amelinckx, G. Van Tendeloo, and J. Van Landuyt: *Mater. Sci. Forum*, 1985, vol. 3, pp. 123–42.
23. P.R. Okamoto and G. Thomas: *Acta Metall.*, 1971, vol. 19, pp. 825–41.
24. A. Arya, S. Banerjee, G.P. Das, I. Dasgupta, T. Saha-Dasgupta, and A. Mookerjee: *Acta Mater.*, 2001, vol. 50, pp. 3575–87.
25. A. Arya, G.K. Dey, V.K. Vasudevan, and S. Banerjee: *Acta Mater.*, 2002, vol. 50, pp. 3301–15.
26. U.D. Kulkarni: *Metall. Mater. Trans. A*, 2002, vol. 33A, pp. 3573–76.
27. P. Hohenberg and W. Kohn: *Phys. Rev.*, 1964, vol. 136, pp. B864–B871.
28. W. Kohn and L.J. Sham: *Phys. Rev.*, 1965, vol. 140, pp. A1133–A1138.
29. O.K. Andersen and O. Jepsen: *Phys. Rev. Lett.*, 1984, vol. 53, pp. 2571–74.
30. O.K. Andersen, O. Jepsen, and M. Sob: in *Electronic Band Structure and Its Applications*, Yussouff M, ed., Lecture Notes in Physics, Springer Verlag, Berlin, 1987, vol. 283, pp. 1–57.
31. O.K. Andersen, O. Jepsen, and G. Krier: in *Lectures on Methods of Electronic Structure Calculations*, V. Kumar, O.K. Andersen, and A. Mookerjee, eds., World Scientific, Singapore, 1994, pp. 63–124.
32. U. von Barth and L. Hedin: *J. Phys.*, 1972, vol. C5, pp. 1629–42.
33. P. Villars and L.D. Calvert: *Pearson*'s Handbook of Crystallographic Data for Intermetallic Phases, ASM, Metals Park, OH, 1985.
34. *Smithells Metals Reference Book*, E.A. Brandes and G.B. Brook, eds., Butterworth-Heinemann, Oxford, United Kingdom, 1998.
35. F.D. Murnaghan: *Proc. Nat. Acad. Sci., USA*, 1944, vol. 30, pp. 244–47.